

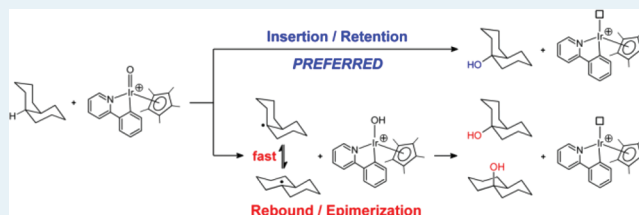
Cp* Iridium Precatalysts for Selective C–H Oxidation via Direct Oxygen Insertion: A Joint Experimental/Computational Study

Meng Zhou,[†] David Balcells,^{*,‡} Alexander R. Parent,[†] Robert H. Crabtree,^{*,†} and Odile Eisenstein^{*,§}[†]Department of Chemistry, Yale University, P.O. Box 208107, New Haven, Connecticut 06520, United States[‡]Department of Chemistry, Universitat Autònoma de Barcelona, 08193 Bellaterra, Barcelona, Catalonia, Spain[§]Institut Charles Gerhardt, Université Montpellier 2, CNRS 5253, cc 15001, Place Eugène Bataillon 34095, Montpellier, France

Supporting Information

ABSTRACT: A series of Cp*Ir complexes are active precatalysts in C–H oxidation of *cis*-decalin, cyclooctane, 1-acetylpyrrolidine, tetrahydrofurans, and γ -lactones. Moderate to high yields were achieved, and surprisingly, high selectivity for mono-oxidation of cyclooctane to cyclooctanone was observed. Kinetic isotope effect experiments in the C–H oxidation of ethylbenzene to acetophenone yield $k_H/k_D = 15.4 \pm 0.8$ at 23 °C and 17.8 ± 1.2 at 0 °C, which are consistent with C–H oxidation being the rate-limiting step with a significant tunneling contribution. The nature of the active species was investigated by TEM, UV–vis, microfiltration, and control experiments. DFT calculations showed that the C–H oxidation of *cis*-decalin by Cp*Ir(ppy)(Cl) (ppy = *o*-phenylpyridine) follows a direct oxygen insertion mechanism on the singlet potential energy surface, rather than the radical rebound route that would be seen for the triplet, in good agreement with the retention of stereochemistry observed in this reaction.

KEYWORDS: iridium, metal oxo, oxene, C–H oxidation, alkane activation, DFT, reaction mechanism, insertion



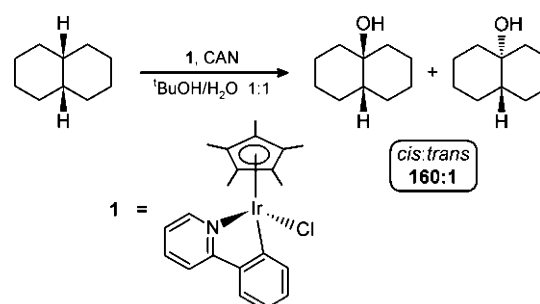
INTRODUCTION

C–H activation^{1–5} plays a growing role in modern chemistry. This reaction is of importance for the efficient functionalization of alkanes,^{6–9} which is needed to transform raw materials like natural gas and oil into feedstock chemicals. Among the methods developed to perform this challenging process, C–H oxidation catalyzed by transition metal complexes is one of the most promising. In one such approach, a high-valent metal–oxo active species^{10–18} is generated *in situ* with a sacrificial oxidant. Metal–oxo complexes of this sort can act as potent oxidizing agents not only in C–H oxidation, but also in alkane desaturation^{19,20} and water oxidation.^{21–32}

We recently reported a series of Cp*Ir (Cp* = C₅Me₅) complexes that are efficient precatalysts for water oxidation.^{33,34} We then showed that some of these complexes are also active in catalytic C–H oxidation.³⁵ With ceric ammonium nitrate, CAN, as sacrificial oxidant, and water as the oxygen source, C–H oxidation of several substrates was achieved under mild conditions with yields up to 72%. Remarkably, the Cp*Ir(ppy)Cl (ppy = *o*-phenylpyridine) precatalyst, **1**, catalyzes the hydroxylation of *cis*-decalin with retention of its stereochemistry (Scheme 1).

The rebound pathway (Scheme 2), the textbook mechanism for C–H oxidation by high-valent metal–oxo complexes, would imply the formation of an Ir(V)=O intermediate in our catalytic system. Originally postulated by Groves,^{36,37} this pathway involves two key steps: (i) H abstraction from the C–H bond by the metal–oxo complex to give M–OH and a

Scheme 1. Cp*Ir-Catalyzed Hydroxylation of *cis*-Decalin with Retention of Stereochemistry



substrate C-centered radical, followed by (ii) the rebound step, in which the OH group is transferred to the radical to form C–OH. The initial H abstraction step may involve tunneling.^{38–41}

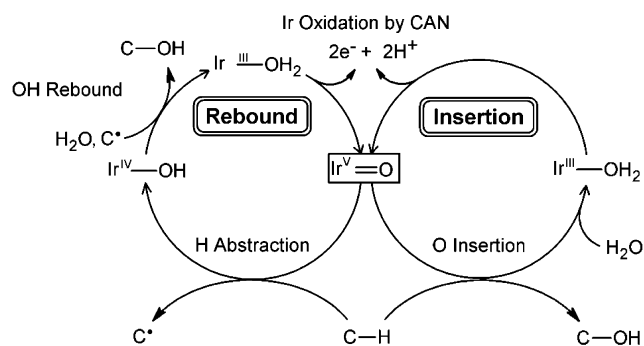
The chemistry of the metal–oxo active species has been studied extensively, both experimentally^{42–55} and theoretically,^{56–67} in relation to methane monooxygenase (MMO) and cytochrome P450 (CYP450) hydroxylases and their biomimetic complexes. Recent studies^{68–72} have shown that the hydroxo intermediate may also give rise to desaturase activity^{73–79} by abstraction of a second H atom adjacent to the initial radical site.

Received: November 14, 2011

Revised: December 27, 2011

Published: December 28, 2011

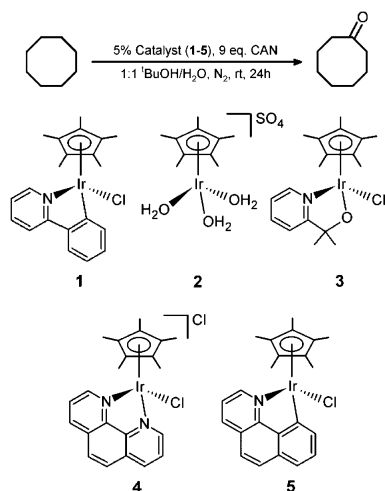
Scheme 2. Alternative Reaction Mechanisms Postulated for Iridium-Catalyzed C–H Oxidation



In our case, the formation of a tertiary radical in the rebound mechanism is expected to give fast *cis*- to *trans*- decalyl radical isomerization, with a rate constant of $>10^8 \text{ s}^{-1}$.⁸⁰ This pathway is inconsistent with the very high stereoretention we observe (Scheme 1). Highly selective hydroxylation has nevertheless been justified in bioinorganic Fe systems by adopting one of two hypotheses: either (1) oxygen rebound is extremely fast, preventing radical rearrangement; or (2) the rebound barrier vanishes if the spin state of the system permits this, and the reaction becomes effectively a direct oxygen atom insertion, in which no rearranging free radicals are formed (Scheme 2). Fast rebound, hypothesis 1, was invoked by Friesner and Lippard to rationalize selective C–H oxidation by MMO,⁸¹ whereas direct O atom insertion, hypothesis 2, was originally proposed by Shaik in his two-state reactivity model for cytochrome P450.^{82–84}

Oxidation catalysis by organometallic species can be hard to interpret because of the possibility that the real catalyst is an oxidation product of the precursor, perhaps involving oxidative degradation of one or more ligands and even formation of a heterogeneous nanoparticulate metal oxide. We have recently obtained quartz crystal nanobalance evidence for the homogeneity of Cp*Ir(2-(2'-pyridyl)-2-propanolate)trifluoroacetate, an analogue of **3** (Scheme 3),⁸⁵

Scheme 3. Cp*Ir Precatalysts for the C–H Oxidation of Cyclooctane



under electrochemical conditions, at least at short times (minutes), and have adopted the model that the present

system derived from precursor **1** is also homogeneous; certainly the high selectivity observed seems much more easily explained in that way.

In this article, we report more detailed experiments on Cp*Ir-catalyzed C–H oxidation with additional precatalysts and substrates. The mechanism has been studied theoretically at the DFT(B3LYP) level. In agreement with the experiments, we propose a direct oxygen insertion pathway in which the substrate is oxidized by an Ir(V)–oxo active species in a closed-shell singlet state, without the participation of radical intermediates. Kinetic isotope effect experiments suggest that significant tunneling effects are involved.

EXPERIMENTAL RESULTS

Cp*Ir-Catalyzed C–H Oxidation. We previously showed that Ir(Cp*)(ppy)(Cl), **1** (Scheme 3) selectively catalyzed the *cis*-decalin hydroxylation with retention of configuration.³⁵ We now report the product *cis*-decalol yield, the percent of recovered starting material (RSM), and mass balance at three time points for the *cis*-decalin hydroxylation catalyzed by **1** (Table 1). The product yield initially increased (10% to 15%)

Table 1. *cis*-Decalin Hydroxylation Catalyzed by **1 over Time^a**

time (h)	yield, ^b %	RSM, ^c %	mass balance, ^d %
2	10	67	77
5	15	45	61
24	7	49	57

^aConditions: 4% **1**, 5 equiv CAN, 10 mL ^tBuOH/H₂O 1:1, rt, N₂, dark, analyzed by GC–FID. ^bYield = product/total starting material. ^cRSM = recovered starting material/total starting material. ^dMass balance = yield + RSM.

but decreased at longer time (15% to 7%), but the mass balance decreased over time (77% to 57%). A control reaction over 11 h without a catalyst gave 61% RSM and no *cis*-decalol or significant amount of other products extractable by organic solvent.

A series of Cp*Ir complexes, **1–5** (Scheme 3), catalyze the oxidation of cyclooctane under the same conditions. With **1**, the substrate is oxidized to cyclooctanone with eight turnovers and 20% yield (Table 2). Precatalyst **2** shows similar but lower

Table 2. Yield and Turnover in Cyclooctane Oxidation Catalyzed by **1–5^a**

precatalyst	1	2	3 ^b	4	5
yield ^c	20%	17%	25% (15%) ^d	3%	8%
turnover	8	7	10	1	3

^aConditions: 5% catalyst loading, 50 μL cyclooctane, 9 equiv CAN in 10 mL 1:1 ^tBuOH/H₂O, under N₂ and at room temperature for 24 h. ^bSide product analysis: cyclooctanol, not detected; 1,2-cyclooctadione, not detected; 1,3-cyclooctadione, <0.1% yield; 1,4-cyclooctadione, <1% yield; 1,5-cyclooctadione, not detected; suberic acid, <1% yield. ^cYield = product/total starting material, by ¹H NMR integration with 1,3,5-trimethoxybenzene as the internal standard. ^dWith 23% RSM by GC–FID.

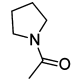
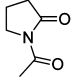
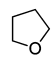
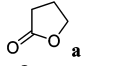
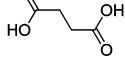
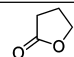
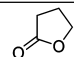
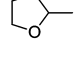
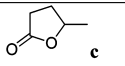
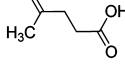
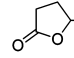
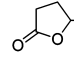
performance. The results improve with **3**, which gives 10 turnovers and 25% yield. Raising the loading of **3**, the amount of CAN, or both did not improve the yield (see the Supporting Information). With cyclooctanone as the starting material under the catalytic oxidation conditions, 8% cyclooctanone was

recovered at the end of the reaction. Precatalysts **4** and **5** are ineffective, giving turnovers below 5 and yields lower than 10%. Without a catalyst, no cyclooctanone or cyclooctanol was detected. Other byproducts, one of which predominated, were detected but could not be identified.

Different byproducts were detected for the reaction catalyzed by **3**, the most efficient precatalyst. Cyclooctanol, thought to arise from the initial oxidation of cyclooctane, was not detected, presumably because of rapid further oxidation to cyclooctanone. The reaction is highly selective for cyclooctanone, and surprisingly, little of the expected double-oxidation product, cyclooctadione, is formed. Neither 1,2- nor 1,5-cyclooctadione was detected, whereas the 1,3 and 1,4 isomers were obtained only in yields below 1%.

Heterocycles containing more reactive C–H bonds were also tested (Table 3). Despite the higher activity of **3**, **2** was

Table 3. C–H Oxidation of Heterocycles with **2**^a

Entry	Substrate	Product (Yield ^b)	Turnover
1		 (90%)	180
2 ^c		 (72%)  (18%)	216
3 ^d		a (51%), b (41%)	266
4 ^e		b (33%)	66
5 ^{e,f}		b (13%)	N/A
6		 (19%)  (78%)	272
7 ^{d,g}		c (20%), d (80%)	280
8 ^e		d (15%)	15
9 ^{e,f}		d (0%)	N/A

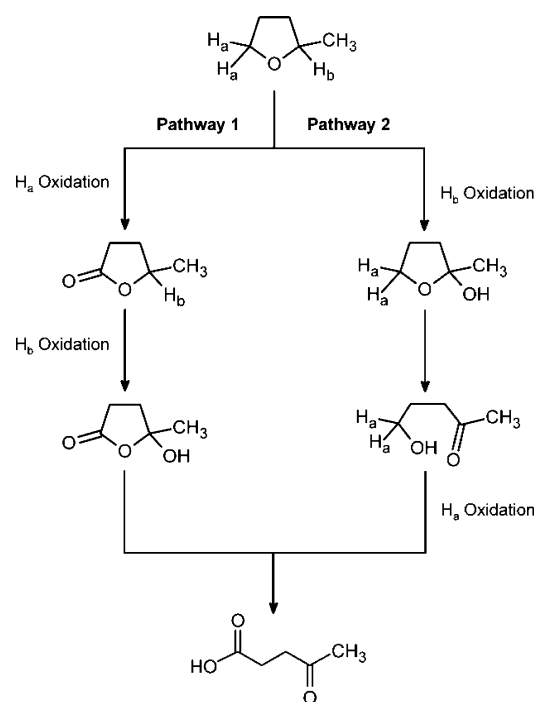
^aConditions: 1% **2**, 8 equiv CAN, 50 μ L substrate, in 10 mL D₂O solvent under N₂, rt, dark, 30 min, unless noted otherwise. ^bYield = product/total starting material, by ¹H NMR integration with 1,3,5-trimethoxybenzene as the internal standard. ^c20 min, in 20 mL D₂O. ^d1 h. ^eMass balance >98%. ^fNo catalyst was used. ^gPrecatalyst **1** was used, and the reaction was not run in the dark.

preferred as the precatalyst because of its ease of synthesis and comparable activity. In most cases, **2** was used at 1% loading, and the reaction was performed in the dark to avoid potential photochemical oxidation by stoichiometric Ce(IV) alone.⁸⁶ Several substrates gave excellent yields. For example, 1-acetylpyrrolidine was converted to 1-acetyl-2-pyrrolidone in 90% yield (entry 1). When pyrrolidine itself was the substrate, however, no product was detected.³⁵ The possibility that the pyrrolidine was binding to the metal and shutting down reactivity was tested by looking at a pyrrolidine-THF mixture, THF being a good substrate. This unexpectedly showed that THF was oxidized in the presence of pyrrolidine (see Supporting Information), so pyrrolidine does not act as a catalyst poison. The oxidation of THF in the presence of

pyrrolidine does not seem consistent with reversible binding of pyrrolidine because we would then expect pyrrolidine to be oxidized, contrary to experiment. Under the conditions of entry 2, THF was oxidized to γ -butyrolactone (**a**) and the over-oxidation product succinic acid (**b**) in 72% and 18% yield, respectively.

When the reaction time was raised from 20 min to an hour (entry 3), the amount of succinic acid formed increased from 18% to 41% yield at the expense of the γ -butyrolactone, which went from 72% to 51% yield, suggesting that γ -butyrolactone was further converted to succinic acid as the reaction continued. We therefore explored the C–H oxidation of pure γ -butyrolactone (entry 4), and indeed, 33% yield of succinic acid was obtained. Control reactions without a catalyst gave less efficient conversion, with the yield decreasing to 13% (entry 5). Unsymmetric 2-methyl THF gave 19% yield of γ -valerolactone (**c**) and 78% levulinic acid (**d**) (see Scheme 4) under the same

Scheme 4. Alternate Pathways in the C–H Oxidation of 2-Methyl THF^a



^aPathway 2 is preferred.

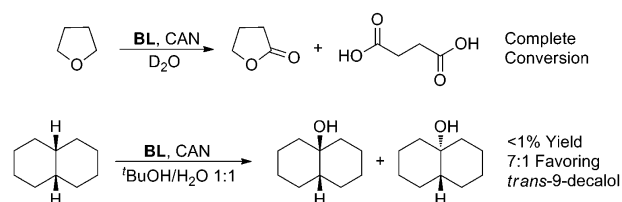
oxidation conditions (entry 6). Precatalyst **1** was similarly effective in this reaction (entry 7). Higher catalytic turnovers were observed for entries 1, 2, 3, 6, and 7 of Table 3, up to 280 in the oxidation of 2-methyl THF, thanks to the higher reactivity of these substrates with respect to cyclooctane.

In view of these results, we explored the oxidation pathway that gave rise to levulinic acid (Table 3 and Scheme 4). Levulinic acid can be thought to form by regioselective oxidation of the secondary C–H (H_a) of 2-methyl THF, followed by further oxidation of the tertiary C–H (H_b) of an initial γ -valerolactone product (pathway 1). Alternatively, it can form by regioselective oxidation of the tertiary C–H (H_b) of 2-methyl THF, followed by the oxidation of the initial oxo-alcohol product to give levulinic acid (pathway 2). We envisioned that pathway 1 would require that C–H oxidation of γ -valerolactone be facile. Experimentally, however, the

sluggish oxidation of γ -valerolactone to levulinic acid (15% yield, entry 8) together with the large amount of levulinic acid (78% yield, entry 6) produced by 2-methyl THF oxidation suggests that γ -valerolactone is not the key intermediate. In addition, no reaction occurred for γ -valerolactone without a catalyst (entry 9). Pathway 2, involving regioselective oxidation of a tertiary C–H, is likely to go faster than pathway 1, involving the oxidation of a CH₂ group, which is typically less reactive.

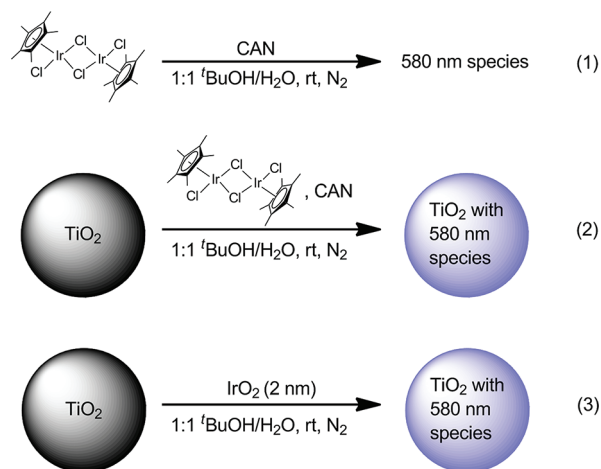
As a control experiment for homogeneity, we showed that a preparation of 25 nm IrO₂ nanoparticles was ineffective as a catalyst for *cis*-decalin hydroxylation.³⁵ We recently reported the anodic deposition of a highly active amorphous heterogeneous water oxidation catalyst from complex **2** on a conductive ITO (indium tin oxide) glass plate (the so-called “blue layer” {IrO_(2-x)} or BL).⁸⁷ We found that the authentically heterogeneous BL catalyst gave complete conversion of THF to γ -butyrolactone and succinic acid in a ratio of 1:0.7, but was ineffective and unselective in *cis*-decalin oxidation (see Supporting Information), despite the high activity of BL in water oxidation (Scheme 5).

Scheme 5. THF and *cis*-Decalin Oxidation by the “Blue Layer” {IrO_(2-x)}



Nature of the Active Species. A UV–vis absorption feature was found at 580 nm (see Supporting Information) in the reaction mixture containing CAN and (Cp*IrCl₂)₂ (eq 1, Scheme 6). The band is in the typical range of that of iridium

Scheme 6. The Formation of the 580 nm Species



oxide particles.^{88,89} An attempted direct TEM study on the solution mixture was unsuccessful because of crystallization of CAN (see Supporting Information). Fortunately, TEM studies can be performed indirectly on the sample because the blue material that corresponds to the 580 nm band irreversibly absorbs onto commercially available 25 nm TiO₂ nanoparticles

(confirmed by UV–vis in the diffuse reflectance mode; see Supporting Information). A blue powder, obtained by stirring the 25 nm TiO₂ in the presence of (Cp*IrCl₂)₂ and CAN (eq 2 Scheme 6) gave a TEM image that did not differ significantly from the starting material 25 nm TiO₂ (see Supporting Information). Given that the detection limit of TEM was 1–2 nm, the result is consistent with the 580 nm species absorbed onto TiO₂ nanoparticles smaller than 2 nm. In addition, a suspension of 2 nm IrO₂ nanoparticles⁸⁹ also gave a blue powder in the presence of 25 nm TiO₂ (eq 3, Scheme 6) and gave similar TEM images. The 580 nm species easily passed through a 220 nm filter.

Similar comparison experiments were carried out for complexes **1** and **3** (see Supporting Information). Complex **3** also produces a 580 nm species in solution, and its TEM image, where the 580 nm species was again absorbed onto TiO₂ nanoparticles, was similar to that from (Cp*IrCl₂)₂. This 580 nm species also passed through the 220 nm filter. Direct TEM study was applied to the filtered (220 nm) solution from complex **3** in the absence of 25 nm TiO₂ particles, but no nanoparticles were observed. Of course, a low concentration of nanoparticles cannot be excluded. In contrast, addition of complex **1** to CAN in solution does not give rise to any significant yield of the 580 nm species (UV–vis), and no color change was observed in added TiO₂ nanoparticles. Control experiments in *cis*-decalin hydroxylation were performed for complexes **1**, **3**, and (Cp*IrCl₂)₂ (see Supporting Information). At the end of the initial 12 h catalytic reaction, when the 580 nm band was present, additional CAN was added to allow for further reaction over 12 h. The effect of the additional CAN was determined by comparison with a separate but identical sample in which no additional CAN was added after the initial 12 h reaction; the reaction time was extended to 24 h to match the comparison sample. After 24 h, both the yield of *cis*-decalol and the amount of recovered starting material were only slightly lower in the case with additional CAN than those in the case without additional CAN, except for precatalyst (Cp*IrCl₂)₂, where the amount of recovered starting material is 10% larger with additional CAN. The results for this part of the study are summarized in Table 4. The 580 nm species therefore does not seem to be a good catalyst.

Kinetic Isotope Effect. Precatalyst **1** was chosen for further study because it does not give the 580 nm species in significant amount, even after 5 h of reaction, and the calculations were also carried out on this species. We previously showed that **1** catalyzes the stereoretentive oxidation of *cis*-decalin to *cis*-9-decalol (Scheme 1). These results suggest that the reaction does not involve radical species. With the aim of shedding light on the reaction mechanism, we performed a kinetic isotope effect (KIE) study. The KIE in the oxidation of ethylbenzene to acetophenone catalyzed by **1** was studied by competitive oxidation of ethylbenzene and deuterated ethylbenzene (Scheme 7, eq 1) with quantitation by ¹H and ²H NMR with MeNO₂ and MeNO₂-d₃ as internal standards (see Supporting Information). The experiments give $k_H/k_D = 15.4 \pm 0.8$ at 23 °C and $k_H/k_D = 17.8 \pm 1.2$ at 0 °C, consistent with C–H oxidation being the rate-limiting step with a significant tunneling contribution.

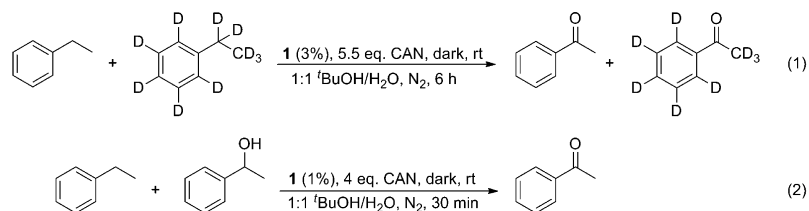
A tunneling-enhanced KIE is normally associated with a low and narrow C–H activation barrier (vide infra). High KIEs have also been observed in ethylbenzene oxidation by synthetic iron heme and nonheme systems.^{90,91} We attributed our KIE to the harder step, initial oxidation of ethylbenzene to *sec*-phenethyl alcohol.

Table 4. Data Relating to the Nature of the Active Species

Cp*Ir complexes and IrO ₂ nanoparticles	results ^a
1	No significant 580 nm band observed with CAN. No color change was seen in the TiO ₂ NPs. No reactivity was detected after 12 h with additional CAN.
(Cp*IrCl ₂) ₂	A 580 nm band was observed with CAN, and the 580 nm species passed through a 220 nm filter. Nanoparticles (>2 nm) were not found by TEM (indirect method by absorption onto TiO ₂ NPs). No reactivity was seen after 12 h with additional CAN.
3	A 580 nm band was observed, and the 580 nm species passed through a 220 nm filter. Nanoparticles (>2 nm) were not found by TEM either by direct observation or via the indirect method with TiO ₂ NPs. No reactivity was seen after 12 h with additional CAN.
IrO ₂ (2 nm NPs)	Shows a 580 nm band that absorbs onto TiO ₂ NPs upon mixing.

^aNP = nanoparticle.

Scheme 7. Kinetic Isotope Effect Experiments



The KIE is expected to be little affected by the subsequent fast oxidation of *sec*-phenethyl alcohol to acetophenone. Indeed, competition experiments (Scheme 7, eq 2) showed that *sec*-phenethyl alcohol oxidation is >3 times faster than that of ethylbenzene (see Supporting Information). In control reactions without catalyst, CAN gave only 7% yield of acetophenone from *sec*-phenethyl alcohol oxidation, but with a 1% loading of **1**, the yield rose to 98% under the same conditions. A higher mass balance (89%) than those of alkane oxidations was obtained for the catalytic oxidation of ethylbenzene to acetophenone. No acetophenone product was found in the ethylbenzene oxidation when air is the terminal oxidant instead of CAN in the presence of **1** (see Supporting Information).

■ COMPUTATIONAL STUDIES

Rebound Mechanism. The reaction mechanism of Cp*Ir-catalyzed C–H oxidation was studied at the DFT(B3LYP) level including the solvent effect (see Computational Details for further information). The results will be discussed by using the potential energies because they are more appropriate to compare the electronic states of the catalyst. This choice is also possible because the pathways being compared have similar molecularity. Consequently, both the potential and Gibbs energies (reported in the Supporting Information) vary in a parallel manner along the reaction pathways.⁹² The remarkable stereoretentive hydroxylation⁹³ of *cis*-decalin to *cis*-9-decalol catalyzed by **1**³⁵ (Scheme 1) is selected as the case study. In the calculations, the experimentally used Cp* ligand is modeled as Cp (see Computational Details). The initial oxidation of the catalyst yields the Ir(V)-oxo complex^{94,95} [IrO(ppy)(Cp)]⁺ (Scheme 2), which is postulated as the model active species. The agreement between experiment and theory is consistent with a homogeneous catalyst rather than a heterogeneous one, such as Ir oxide or BL nanoparticles. As discussed above, we used these materials in control reactions without seeing activity and selectivity for *cis*-decalin.

The singlet, **S**; triplet, **T**; and quintet, **Q**, states of the model active species are optimized. **T** has the lowest energy, with **S** and **Q** being 2.3 and 43.0 kcal mol⁻¹ higher, respectively. Both **S** and **T** are thus accessible and may hydroxylate *cis*-decalin,

whereas **Q** is excluded because of its high energy. The Ir(V)-oxo moiety of **T** has a local spin density of 1.81, which is more than 90% of the total. Most of this spin density, 1.16, accumulates upon the oxygen atom, thus showing that the oxo ligand has strong radical character, also known as oxyl character. Oxyl character promotes C–H oxidation through the rebound mechanism (Scheme 2), as shown in previous studies by us^{96–98} and others.^{99–102}

The hydroxylation of *cis*-decalin by **T** starts with radical H abstraction. In the weak prereaction complex,¹⁰³ *cis*-**T-1**, which is 3.9 kcal mol⁻¹ below reactants (Figure 1), the oxygen of **T** makes a H-bond with the substrate; $d(\text{O}\cdots\text{H}) = 2.85 \text{ \AA}$. In the transition state, *cis*-**T-TS1** (Figure 2), the C–H involved in the H-bond of *cis*-**T-1** is cleaved, and the H is transferred to the oxyl group; $d(\text{H}\cdots\text{C}) = 1.32 \text{ \AA}$, $d(\text{O}\cdots\text{H}) = 1.27 \text{ \AA}$. The relaxation of *cis*-**T-TS1** to products yields the hydroxo intermediate *cis*-**T-2**; $d(\text{IrO-H}) = 1.01 \text{ \AA}$. In this species, the organic fragment has a local charge and spin density of 0.05 and 0.93, respectively, and it can be thus formulated as the neutral decalyl radical (C₁₀H₁₇[•]). The hydrogen abstraction step, *cis*-**T-1** → *cis*-**T-TS1** → *cis*-**T-2**, has a low energy barrier, $\Delta E^\ddagger = 12.4 \text{ kcal mol}^{-1}$, and is exothermic, $\Delta E = -2.1 \text{ kcal mol}^{-1}$.

After H abstraction, the decalyl radical in *cis*-**T-2** may be oxidized to *cis*-9-decalol by OH rebound (Figure 3). In the transition state, *cis*-**T-TS2** (Figure 3), the hydroxo ligand is transferred from the metal to the radical; $d(\text{Ir}\cdots\text{OH}) = 2.04 \text{ \AA}$, $d(\text{C}\cdots\text{OH}) = 2.41 \text{ \AA}$. On the reactant side, *cis*-**T-TS2** is connected to the hydroxo complex *cis*-**T-2'**. The main difference between this species and the H abstraction product, *cis*-**T-2**, arises from a change in the orientation of the OH ligand. This suggests that the rebound step requires a proper orientation of the OH ligand relative to the radical.^{72,104,105} The relaxation of the transition state toward products yields intermediate *cis*-**T-3**, in which the *cis*-9-decalol product is formed and O-bound to Ir; $d(\text{Ir-OH}) = 2.54 \text{ \AA}$, $d(\text{C-OH}) = 1.52 \text{ \AA}$. The OH rebound step, *cis*-**T-2'** → *cis*-**T-TS2** → *cis*-**T-3**, involves a significant energy barrier, $\Delta E^\ddagger = 9.3 \text{ kcal mol}^{-1}$, and is much more exothermic than H abstraction, $\Delta E = -27.3 \text{ kcal mol}^{-1}$.

Before OH rebound takes place, *cis*-**T-2'** is expected to rearrange to *trans*-**T-2'** by *cis* → *trans* isomerization of the

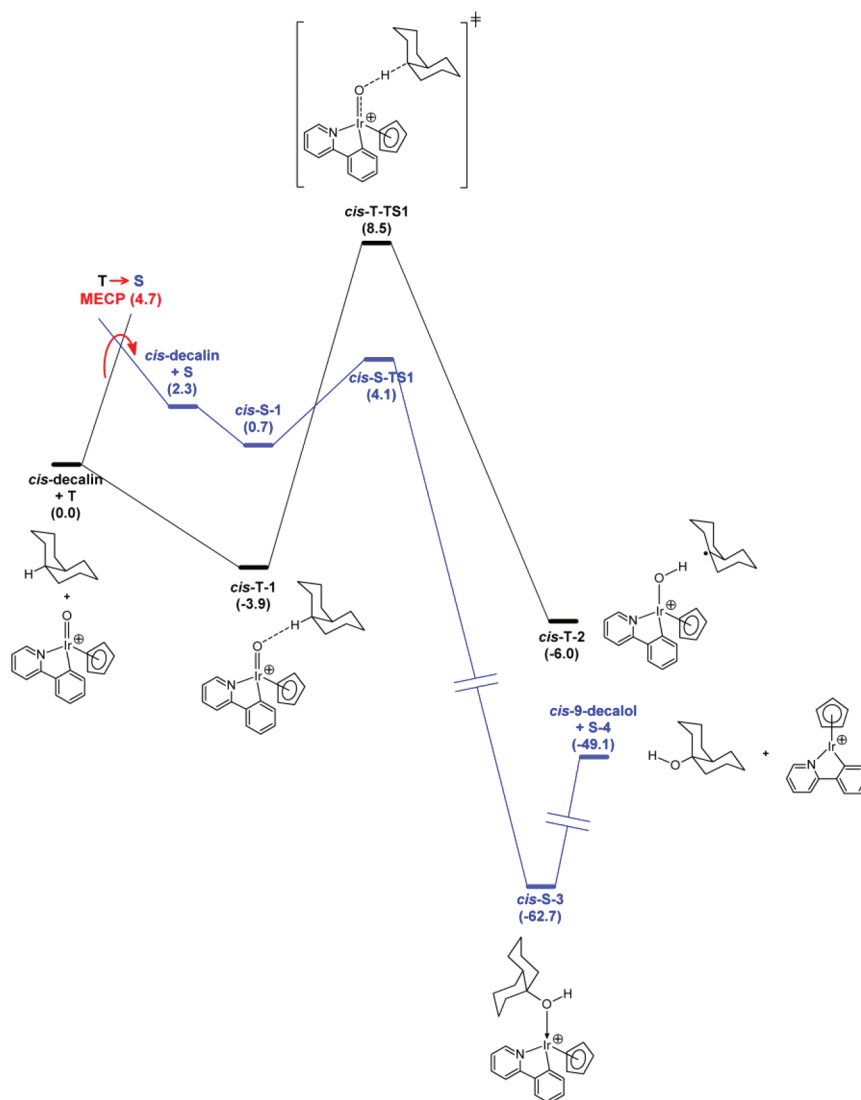


Figure 1. Energy profiles, in kcal mol⁻¹, for the C–H oxidation of *cis*-decalin in the triplet (black) and singlet (blue) states, with the MECP (minimum energy crossing point) between the singlet and triplet surfaces.

decalyl radical, which is extremely fast, $k > 10^8 \text{ s}^{-1}$.⁸⁰ OH rebound from *trans*-T-2' yields the *trans*-9-decalol product (Figure 3) through the transition state *trans*-T-TS2 (Figure 2) and the intermediate *trans*-T-3. The geometrical parameters associated with the bonds being cleaved and formed in this pathway, Ir–O and O–C, are very similar to those found in the *cis* pathway. However, the whole *trans* pathway runs at lower energy than the *cis*. The energy differences between these pathways are significant: 3.5 kcal mol⁻¹ for the reactant, 2.6 kcal mol⁻¹ for the transition state, and 2.5 kcal mol⁻¹ for the product, all favoring the formation of *trans*-9-decalol, which is the minor experimental product. The final decoordination of this alcohol from iridium has an energy cost of $\sim 7 \text{ kcal mol}^{-1}$ and yields T-4. From T-4, the active species, T, would be recovered by binding of water and Ir(III) \rightarrow Ir(V) oxidation (Scheme 2).

Oxygen Insertion Mechanism. The singlet state of [IrO(ppy)(Cp)]⁺ is only 2.3 kcal mol⁻¹ above the triplet and is thus energetically accessible. Unlike T, S does not have the oxyl character needed for radical H abstraction. Nevertheless, S promotes the reaction by oxygen insertion (Scheme 2). This reaction is initiated by the formation of *cis*-S-1, in which the

Ir(V)-oxo moiety is H-bonded to a tertiary C–H of the substrate (Figure 1). *cis*-S-1 is connected with the transition state *cis*-S-TS1 (Figure 2), in which the C–H making the H-bond is cleaved to transfer the H atom to the oxo ligand; $d(\text{H}\cdots\text{C}) = 1.15 \text{ \AA}$, $d(\text{O}\cdots\text{H}) = 1.59 \text{ \AA}$. This transition state was located by reoptimizing *cis*-T-TS1 in the singlet state and by careful examination of the imaginary frequency and IRC calculations. The geometries of *cis*-S-TS1 and *cis*-T-TS1 are similar, with the former being more reactant-like, since the C–H bond is hardly elongated. The relaxation of *cis*-S-TS1 toward products leads directly to *cis*-S-3, in which the *cis*-9-decalol product is already formed and coordinated to Ir through O; $d(\text{C}-\text{O}) = 1.54 \text{ \AA}$, $d(\text{O}-\text{H}) = 0.98 \text{ \AA}$, $d(\text{Ir}-\text{O}) = 2.20 \text{ \AA}$.

The barrier for the oxygen insertion pathway, *cis*-S-1 \rightarrow *cis*-S-TS1 \rightarrow *cis*-S-3, is only 3.4 kcal mol⁻¹. The overall hydroxylation reaction (Figures 1 and 3) is much more exothermic in the singlet state, $\Delta E = -49.1 \text{ kcal mol}^{-1}$, than in the triplet, $\Delta E = -26.3 \text{ kcal mol}^{-1}$ (*cis*) and $\Delta E = -27.2 \text{ kcal mol}^{-1}$ (*trans*). The oxygen insertion mechanism has been also studied for methane, the most inert of the alkanes. In this case, however, the reaction involves a much higher energy barrier, $\Delta E^\ddagger = 25.7 \text{ kcal mol}^{-1}$ (see the Supporting Information for

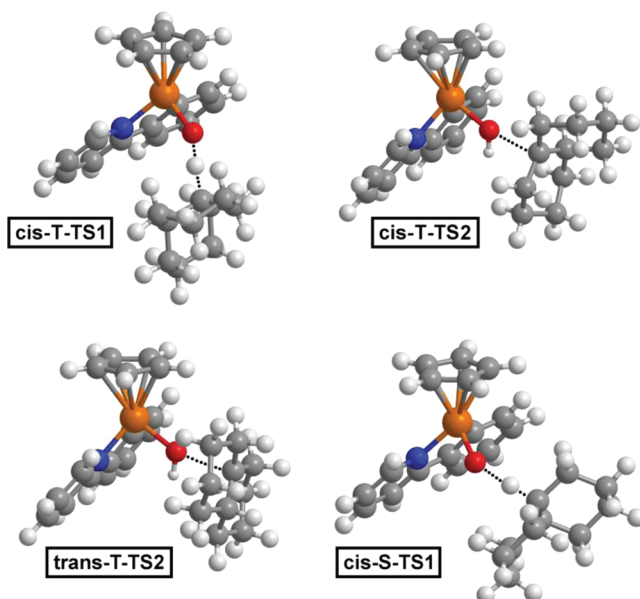


Figure 2. Optimized geometries of the transition states. See Figure 1 for labels.

further details). So far, there is no experimental evidence that methane can be oxidized by the precatalysts used in this study.

The transition state for oxygen insertion in the singlet state is lower than the highest transition state for the two-step rebound pathway in the triplet state. Thus, it could be a mechanism of choice if the triplet-to-singlet intersystem crossing is accessible. The feasibility of this process is estimated from the energy of the minimum energy crossing point (MECP), which is determined by the computational method of Harvey et al.^{106–109} An MECP of 4.7 kcal mol⁻¹ above T was located for the T → S intersystem crossing. The low energy of the MECP, similar to that of *cis-S-TS1*, suggests that the concerted oxygen insertion involves a lower energy pathway when compared with the OH rebound mechanism. The singlet and triplet surfaces may also cross before the transition state for C–H activation. This MECP, whose calculation is very challenging, should be similar to the first MECP, since the metal fragments at these two points have rather similar structures. Therefore, we conclude that the reaction can occur on the singlet state surface.

DISCUSSION

Experimental Section. In the catalytic *cis*-decalin hydroxylation with **1**, the initial increase in the yield of product *cis*-decalol followed by its decrease is consistent with product overoxidation. The decrease in mass balance over time corroborates this hypothesis. Although CAN acting alone without a catalyst did not produce *cis*-decalol or significant amounts of other products extractable by our procedure, we saw only 61% recovered starting material, suggesting that CAN alone does react to a significant extent with *cis*-decalin. This significant background reaction by CAN likely explains why the catalytic reaction consumed the starting material while not producing *cis*-decalol product. In cyclooctane oxidation, where more equivalents of CAN are present, the effect of overoxidation is more prominent. With complex **3**, when 15% yield of product cyclooctanone was obtained, only 23% starting material was recovered, suggesting high conversion of starting material but low yield of product obtainable from the organic layer by our

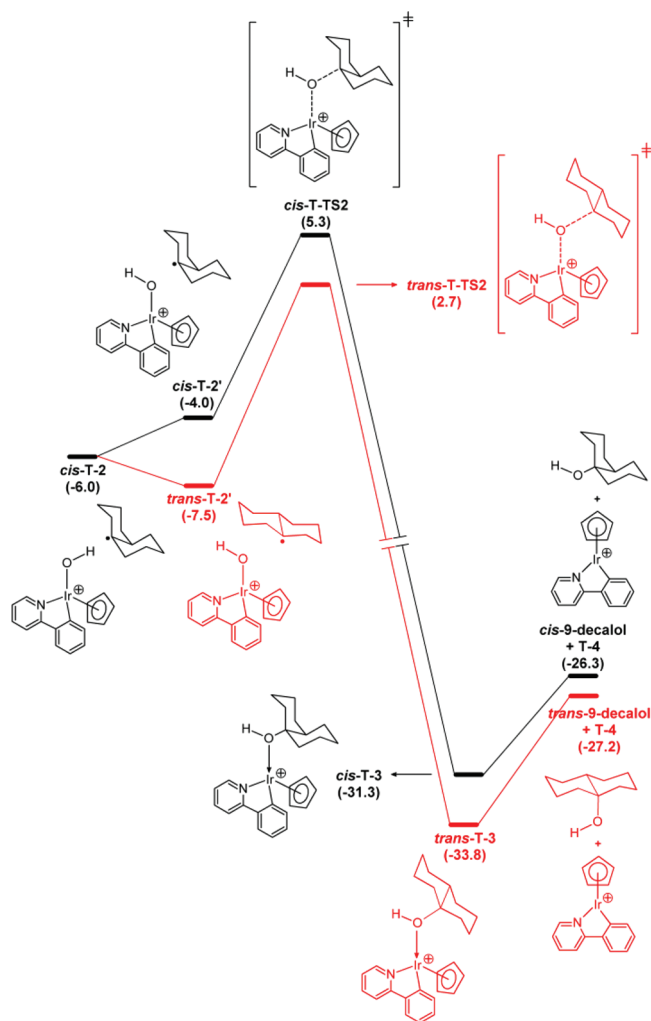


Figure 3. Energy profiles, in kcal mol⁻¹, for *cis* (black) and *trans* (red) rebound in the triplet state.

procedure. Cyclic ketones such as cyclohexanone and cyclopentanone undergo oxidative C–C cleavage with CAN,¹¹⁰ therefore, the product cyclooctanone is most likely consumed as the reaction proceeds. In addition, CAN on its own reacted with cyclooctane but no cyclooctanone or cyclooctanol was produced. The catalytic reaction was more selective than the uncatalyzed one, however. In contrast, the mass balance for catalytic ethylbenzene oxidation is high, 89%, and KIE values were obtained via this reaction.

Catalytic oxidation of heterocycles, containing weaker C–H bonds than those of alkane,^{111,112} gave better yield and turnover number. Oxidative transformations of heterocycles can be useful for organic synthesis.¹⁷ The precatalyst is far more active for THF than for butyrolactone, perhaps because the C–H bonds α to oxygen in the lactone are less reactive with the proposed electrophilic oxo intermediate. For example, after 20 min, 72% lactone and 18% succinic acid were formed from THF, but with butyrolactone as starting material under identical conditions after 30 min, only 33% yield of succinic acid was seen. Control experiments in the absence of Ir gave 13% yield of acid from butyrolactone as substrate as a result of the oxidation by CAN only.

To investigate the active species involved in the catalytic reaction, we tested relevant and known heterogeneous

catalysts.¹¹³ We found that neither 25 nm IrO₂ nanoparticles nor BL was active and selective for *cis*-decalin hydroxylation, even though BL is capable of catalyzing the oxidation of THF (containing weaker C–H bonds^{111,112}). This contrasts with what we found for the Cp*Ir precatalysts.

A band near 580 nm in the UV–vis was found in the catalytic reaction mixture with (Cp*IrCl₂)₂ and complex 3, but not significantly with 1. This means we cannot exclude the formation of small IrO_x particles^{88,89} from all the Cp*Ir precatalysts tested, except 1. The activity of 1 without the appearance of the 580 nm material shows that C–H oxidation can occur without formation of this as yet unidentified species. TEM and microfiltration at 220 nm suggests that any particulate species is <2 nm in diameter. Control experiments showed that after 12 h, no catalytic activity was seen when additional CAN was added, which indicates that the presence of the 580 nm species is not necessarily associated with alkane oxidation. We tentatively interpret the observations from 3 and (Cp*IrCl₂)₂ as consistent with the formation of an IrO_x nanocluster (<2 nm) that is inactive for catalysis of *cis*-decalin hydroxylation. However, we cannot exclude smaller clusters being formed at an early stage of the reaction that are more reactive than the ones present at the end of the reaction.¹¹³ A proposed Ir(IV) aqua complex,¹¹⁴ having a 584 nm band in the UV–vis spectrum, is another attractive candidate for the observed 580 nm feature in our systems.

Theoretical. In the singlet state of the active species, S, the HOMO and LUMO are the antibonding π^* orbitals associated with the Ir=O multiple bond (Figure 4). These $\pi^*(\text{Ir}=\text{O})$

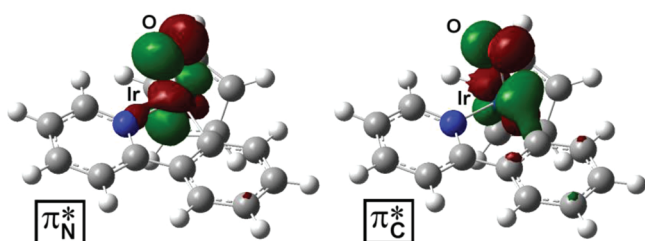


Figure 4. The antibonding $\pi^*_N(\text{Ir}=\text{O})$ and $\pi^*_C(\text{Ir}=\text{O})$ orbitals of $[\text{IrO}(\text{ppy})(\text{Cp})]^+$.

orbitals are perpendicular to the Ir(ppy) plane; the HOMO is oriented along the Ir–N bond, π^*_N , whereas the LUMO is oriented along the Ir–C bond, π^*_C . These orbitals are the out-of-phase combinations of the metal d_π orbitals with the oxygen p_π lone pairs. In the triplet state, T, π^*_N and π^*_C are the SOMOs, each being occupied by a single electron. The S and T states have different occupation of the same antibonding $\pi^*(\text{Ir}=\text{O})$ orbitals and are therefore close in energy; the electronic configuration of S is $(\pi^*_N)^2(\pi^*_C)^0$, whereas that of T is $(\pi^*_N)^1(\pi^*_C)^1$. C–H oxidation by S and T is promoted by the presence of low-energy electron vacancies in these $\pi^*(\text{Ir}=\text{O})$ orbitals, which make the IrO moiety electrophilic. In addition, the double and single occupation of $\pi^*(\text{Ir}=\text{O})$ in S and T, respectively, weakens and activates the Ir=O bond. However, each spin state promotes C–H oxidation by a different reaction mechanism. The singlet state, S, as a closed-shell species, involves a direct oxygen insertion mechanism, whereas the triplet state, T, as an open-shell species, involves an OH rebound mechanism.

The significant contribution of oxygen to the SOMOs of T accounts for the radical oxyl character of this species. This

radical oxyl promotes C–H oxidation through the oxygen rebound mechanism (Figures 1–3), in which electrons are transferred one by one. Ir(V) is first reduced to Ir(IV) by H abstraction and then to Ir(III) by OH rebound. Unlike T, which has two one-electron holes in its SOMOs, S has one two-electron hole in its low-lying LUMO. Therefore, S may oxidize the substrate by accepting two electrons in a single step, in which Ir(V) is directly reduced to Ir(III). This mechanism, which is supported by the calculations (Figure 1), is described as a direct oxygen insertion mechanism because the oxygen of S inserts into the C–H bond of the substrate in a single concerted step. Privalov proposed a similar mechanism for C–H oxidation by a closed-shell $\text{Re}^{\text{VII}}\text{OO}$ peroxo species, in the methyltrioxorhenium catalytic system.¹¹⁵ We believe that the unique reactivity of S stems from its characteristic electronic configuration, in which one of the two $\pi^*(\text{Ir}=\text{O})$ orbitals, π^*_N , is doubly occupied at the HOMO level, whereas the other, π^*_C , is a low-lying LUMO. S is, indeed, isolobal with singlet oxygen, which, having two degenerate $\pi^*(\text{O}=\text{O})$ orbitals, one filled and one empty, also inserts into C–H bonds.¹¹⁶

Despite the extremely fast *cis* → *trans* isomerization of the decalyl radical, $k > 10^8 \text{ s}^{-1}$,⁸⁰ the rebound mechanism could in principle yield the high selectivity observed in our experiments if the energy barrier for OH rebound was either very low or, depending on the spin state, nonexistent.^{81–84} However, the calculations exclude this scenario because the rebound barrier is found to be significant, 9.3 kcal mol^{−1}, only 3.1 kcal mol^{−1} lower than that of H abstraction (Figures 1 and 3). In addition, OH rebound is more favorable in the *trans* pathway than in the *cis*, both thermodynamically and kinetically. Therefore, if the reaction had occurred in the triplet state via the rebound mechanism, the product would have been either *trans*-9-decalol or, at best, a *trans*-9-decalol/*cis*-9-decalol mixture, with the *trans* isomer predominating. This prediction does not fit the experiments, in which *cis*-9-decalol is the major product, thus suggesting that the reaction operates through a different mechanism.

In the singlet state, *cis*-decalin undergoes stereoretentive hydroxylation to *cis*-9-decalol by S because the direct oxygen insertion mechanism does not involve radical intermediates (Figure 1). To take an organic analogy, singlet carbenes, which have an electronic configuration similar to that of S, undergo C–H insertion with retention of configuration.^{117,118} As in the two-state reactivity model proposed by Shaik for $\text{Fe}^{\text{IV}}\text{O}$,^{119,120} the oxidation of *cis*-decalin by $[\text{IrO}(\text{ppy})(\text{Cp})]^+$ may follow two competitive mechanisms, each yielding different reaction products, depending on the spin state of the system: the singlet pathway yields *cis*-9-decalol, whereas the triplet yields *trans*-9-decalol.

The experimental *cis*/*trans* product ratio may be determined by the energy difference between the transition states for oxygen insertion, *cis*-S-TS1, and H abstraction, *cis*-T-TS1. The calculations predict that this energy difference equals 4.4 kcal mol^{−1}, reasonably close to 3.0 kcal mol^{−1}, which is the value that, assuming a Boltzmann distribution at room temperature (298 K), yields the 160:1 *cis*/*trans* ratio observed in the experiments.³⁵ Alternatively, if the reaction starts in the triplet state and finishes in the singlet, the selectivity of the reaction may be controlled by the intersystem crossing rate.

A remarkable feature of oxygen insertion is the very low energy barrier involved in this pathway, $\Delta E^\ddagger = 3.4 \text{ kcal mol}^{-1}$. This barrier is much lower than that found for H abstraction in the rebound mechanism, $\Delta E^\ddagger = 12.4 \text{ kcal mol}^{-1}$. In addition, the

oxygen insertion transition state— $d(\text{H}\cdots\text{C}) = 1.15 \text{ \AA}$, $d(\text{O}\cdots\text{H}) = 1.59 \text{ \AA}$ —is more reactant-like than the H abstraction one: $d(\text{H}\cdots\text{C}) = 1.32 \text{ \AA}$, $d(\text{O}\cdots\text{H}) = 1.27 \text{ \AA}$. This suggests that the energy barrier for oxygen insertion is not only lower but also narrower than that of H abstraction. Nonclassical KIE due to tunneling^{121–123} would be therefore expected if oxygen insertion is the operative mechanism in this reaction.¹²⁴ In line with this, large $k_{\text{H}}/k_{\text{D}}$ values, up to 17.8 ± 1.2 at 0 °C, are found in our experiments (vide supra). This gives further support to the predominance of the retention insertion pathway over the epimerization rebound pathway.

CONCLUSIONS

Cp*Ir complexes selectively catalyze the oxidation of a variety of organic substrates, such as *cis*-decalin to *cis*-9-decalol, cyclooctane to cyclooctanone, 1-acetylpyrrolidine to 1-acetyl-2-pyrrolidone, tetrahydrofurans to γ -lactones, and γ -lactones to carboxylic acids. The large kinetic isotope effect in ethylbenzene oxidation is consistent with C–H oxidation being the rate-limiting step with a significant tunneling contribution. TEM, UV–vis, microfiltration and control experiments for 3 and (Cp*IrCl₂)₂ do not allow us to exclude the formation of iridium oxide particles (580 nm species) that are <2 nm in diameter or an Ir(IV) aqua complex and are not active for *cis*-decalin hydroxylation after 12 h. However, we cannot rule out that particles active for alkane oxidation are formed in the initial stage of the reaction. No significant 580 nm species was observed for **1**, however, so this catalyst is regarded as authentically homogeneous under our conditions. The mechanism of stereoretentive C–H hydroxylation of *cis*-decalin was studied by DFT calculations in which a direct oxygen insertion pathway is found to be more favorable than radical rebound, in line with the experiments.

COMPUTATIONAL DETAILS

Calculations were performed at the DFT level, by using two distinct hybrid functionals: the B3LYP,^{125–127} as implemented in Gaussian03,¹²⁸ to optimize the geometries and compute the frequencies; and the M06,^{129,130} as implemented in Gaussian09,¹³¹ to refine the energies. The B3LYP calculations were carried out with basis set I (Stuttgart–Bonn scalar relativistic ECP with associated basis set for Ir,^{132,133} and the all-electron 6-31G for N, O, C, and H¹³⁴). All geometries were fully optimized at this level of theory without any symmetry or geometry constraints. The nature of all stationary points was confirmed by the analytical calculation of their frequencies, which showed no imaginary frequencies for the minima and a single imaginary frequency for the transition states. The intermediates connected to each transition state were determined by means of IRC calculations.^{135,136} The zero-point, thermal, and entropy energy corrections were determined with basis set I by calculating the Gibbs energy within the harmonic approximation for vibrational frequencies. These corrections are given in the Supporting Information. The energy of the optimized geometries was refined by M06 single point calculations with basis set II (the same as I but with polarization functions added to Ir and the all-electron 6-311++G** for N, O, C, and H^{137–141}). Solvation effects were also introduced in these calculations by using the parametrized continuum SMD model.^{142,143} All energies given and discussed in the text were computed at the M06/SMD/6-311++G** level. Local charges and spin densities were obtained from NPA (natural

population analysis) calculations.¹⁴⁴ The MECP calculations were carried out with the program developed by J. N. Harvey.¹⁴⁵

ASSOCIATED CONTENT

Supporting Information

Experimental setup and product analysis. References for the synthesis and characterization of Cp*Ir precatalysts. UV–vis spectra and TEM images. Full list of authors for references 6, 128, and 131. Optimized geometries and energies of all stationary points reported in the text, plus the MECP and the calculations on the activation of methane. This information is available free of charge via the Internet at <http://pubs.acs.org/>.

AUTHOR INFORMATION

Corresponding Author

*E-mail: david.balcells@uab.cat (D.B.), robert.crabtree@yale.edu (R.H.C.), odile.eisenstein@univ-montp2.fr (O.E.).

ACKNOWLEDGMENTS

This material is based in part upon work supported by the Center for Catalytic Hydrocarbon Functionalization, an Energy Frontier Research Center funded by the U.S. Department of Energy, Office of Science, Office of Basic Energy Sciences under Award Number DE-SC0001298 (M.Z., experimental work) and by DE-FG02-84ER13297 (R.H.C., summer support), and by the NSF GRFP and the Division of Chemical Sciences, Geosciences, and Biosciences, Office of Basic Energy Sciences of the U.S. Department of Energy (DE-FG02-07ER15909) (A.R.P. and G.W.B., spectroscopy). D.B. (computation) thanks the Spanish MICINN for his Juan de la Cierva position. O.E. (computation) thanks the CNRS and the Ministère de l'Enseignement Supérieur et de la Recherche for funding. We thank J. F. Hull (Brookhaven National Laboratory), N. D. Schley, J. D. Blakemore, and Ulrich Hintermair (Yale University) for helpful discussions; Barry Piekos (Yale University) for assistance in TEM measurements; and the Anastas Lab (Yale University) for using their GC–FID.

REFERENCES

- (1) Goldberg, K. I.; Goldman, A. S., Eds.; *Activation and Functionalization of C–H Bonds*; ACS Symposium Series 885; American Chemical Society: Washington, DC, 2004.
- (2) *Chemical Reviews* Thematic Issue on “Selective Functionalization of C–H Bonds”. Crabtree, R. H. *Chem. Rev.* **2010**, *110*, 575.
- (3) Crabtree, R. H. *J. Chem. Soc., Dalton Trans.* **2001**, 2437–2450.
- (4) Labinger, J. A.; Bercaw, J. E. *Nature* **2002**, *417*, 507–514.
- (5) Arndtsen, B. A.; Bergman, R. G.; Mobley, T. A.; Peterson, T. H. *Acc. Chem. Res.* **1995**, *28*, 154–162.
- (6) Arakawa, H.; et al. *Chem. Rev.* **2001**, *101*, 953–996.
- (7) Periana, R. A.; Taube, D. J.; Evitt, E. R.; Löffler, D. G.; Wentrcek, P. R.; Voss, G.; Masuda, T. *Science* **1993**, *259*, 340–343.
- (8) Periana, R. A.; Taube, D. J.; Gamble, S.; Taube, H.; Satoh, T.; Fujii, H. *Science* **1998**, *280*, 560–564.
- (9) Shilov, A. E.; Shul'pin, G. B. *Chem. Rev.* **1997**, *97*, 2879–2932.
- (10) Meunier, B., Ed.; *Biomimetic Oxidations Catalyzed by Transition Metal Complexes*; Imperial College Press: London, 2000.
- (11) Zhang, R.; Newcomb, M. *Acc. Chem. Res.* **2008**, *41*, 468–477.
- (12) Que, L. *Acc. Chem. Res.* **2007**, *40*, 493–500.
- (13) Meunier, B. *Chem. Rev.* **1992**, *92*, 1411–1456.
- (14) Jin, N.; Ibrahim, M.; Spiro, T. G.; Groves, J. T. *J. Am. Chem. Soc.* **2007**, *129*, 12416–12417.
- (15) Bell, S. R.; Groves, J. T. *J. Am. Chem. Soc.* **2009**, *131*, 9640–9641.

- (16) Song, W. J.; Seo, M. S.; George, S. D.; Ohta, T.; Song, R.; Kang, M. J.; Tosha, T.; Kitagawa, T.; Solomon, E. I.; Nam, W. *J. Am. Chem. Soc.* **2007**, *129*, 1268–1277.
- (17) Zhou, M.; Crabtree, R. H. *Chem. Soc. Rev.* **2011**, *40*, 1875–1884.
- (18) Verat, A. Y.; Fan, H. J.; Pink, M.; Chen, Y. S.; Caulton, K. G. *Chem.—Eur. J.* **2008**, *14*, 7680–7686.
- (19) Bigi, M. A.; Reed, S. A.; White, M. C. *Nat. Chem.* **2011**, *3*, 216–222.
- (20) Usharani, D.; Janardanan, D.; Shaik, S. *J. Am. Chem. Soc.* **2011**, *133*, 176–179.
- (21) Siegbahn, P. E. M. *Acc. Chem. Res.* **2009**, *42*, 1871–1880.
- (22) Romain, S.; Vigarà, L.; Llobet, A. *Acc. Chem. Res.* **2009**, *42*, 1944–1953.
- (23) Concepcion, J. J.; Jurss, J. W.; Brennaman, M. K.; Hoertz, P. G.; Patrocinio, A. O. T.; Iha, N. Y. M.; Templeton, J. L.; Meyer, T. J. *Acc. Chem. Res.* **2009**, *42*, 1954–1965.
- (24) Geletii, Y. V.; Besson, C.; Hou, Y.; Yin, Q. S.; Musaev, D. G.; Quinonero, D.; Cao, R.; Hardcastle, K. I.; Proust, A.; Kogerler, P.; Hill, C. L. *J. Am. Chem. Soc.* **2009**, *131*, 17360–17370.
- (25) Kuznetsov, A. E.; Geletii, Y. V.; Hill, C. L.; Morokuma, K.; Musaev, D. G. *J. Am. Chem. Soc.* **2009**, *131*, 6844–6854.
- (26) Nocera, D. G. *Inorg. Chem.* **2009**, *48*, 10001–10017.
- (27) Dempsey, J. L.; Esswein, A. J.; Manke, D. R.; Rosenthal, J.; Soper, J. D.; Nocera, D. G. *Inorg. Chem.* **2005**, *44*, 6879–6892.
- (28) Kohl, S. W.; Weiner, L.; Schwartsburd, L.; Konstantinovski, L.; Shimon, L. J. W.; Ben-David, Y.; Iron, M. A.; Milstein, D. *Science* **2009**, *324*, 74–77.
- (29) Sproviero, E. M.; Gascon, J. A.; McEvoy, J. P.; Brudvig, G. W.; Batista, V. S. *Coord. Chem. Rev.* **2008**, *252*, 395–415.
- (30) Cady, C. W.; Crabtree, R. H.; Brudvig, G. W. *Coord. Chem. Rev.* **2008**, *252*, 444–455.
- (31) Limburg, J.; Vrettos, J. S.; Liable-Sands, L. M.; Rheingold, A. L.; Crabtree, R. H.; Brudvig, G. W. *Science* **1999**, *283*, 1524–1527.
- (32) Shimazaki, Y.; Nagano, T.; Takesue, H.; Ye, B. H.; Tani, F.; Naruta, Y. *Angew. Chem., Int. Ed.* **2004**, *43*, 98–100.
- (33) Hull, J. F.; Balcells, D.; Blakemore, J. D.; Incarvito, C. D.; Eisenstein, O.; Brudvig, G. W.; Crabtree, R. H. *J. Am. Chem. Soc.* **2009**, *131*, 8730–8731.
- (34) Blakemore, J. D.; Schley, N. D.; Balcells, D.; Hull, J. F.; Olack, G. W.; Incarvito, C. D.; Eisenstein, O.; Brudvig, G. W.; Crabtree, R. H. *J. Am. Chem. Soc.* **2010**, *132*, 16017–16029.
- (35) Zhou, M.; Schley, N. D.; Crabtree, R. H. *J. Am. Chem. Soc.* **2010**, *132*, 12550–12551.
- (36) Groves, J. T.; McClusky, G. A. *J. Am. Chem. Soc.* **1976**, *98*, 859–861.
- (37) Groves, J. T. *J. Chem. Educ.* **1985**, *62*, 928–931.
- (38) de Visser, S. P.; Oglario, F.; Sharma, P. K.; Shaik, S. *J. Am. Chem. Soc.* **2002**, *124*, 11809–11826.
- (39) Wang, Q.; Sheng, X.; Horner, J. H.; Newcomb, M. *J. Am. Chem. Soc.* **2009**, *131*, 10629–10636.
- (40) Klinker, E. J.; Shaik, S.; Hirao, H.; Que, L. *Angew. Chem., Int. Ed.* **2009**, *48*, 1291–1295.
- (41) Lehnert, N.; Solomon, E. I. *J. Biol. Inorg. Chem.* **2003**, *8*, 294–305.
- (42) Ortiz de Montellano, P. R. *Chem. Rev.* **2010**, *110*, 932–948.
- (43) Ortiz de Montellano, P. R. *Cytochrome P450: Structure, Mechanism, and Biochemistry*, 3rd ed.; Kluwer Academic/Plenum Publishers: New York, 2005.
- (44) Friedle, S.; Reisner, E.; Lippard, S. J. *Chem. Soc. Rev.* **2010**, *39*, 2768–2779.
- (45) Dey, A.; Jiang, Y. I.; Ortiz de Montellano, P. R.; Hodgson, K. O.; Hedman, B.; Solomon, E. I. *J. Am. Chem. Soc.* **2009**, *131*, 7869–7878.
- (46) Que, L.; Tolman, W. B. *Nature* **2008**, *455*, 333–340.
- (47) Groves, J. T. *J. Inorg. Biochem.* **2006**, *100*, 434–447.
- (48) Tshuva, E. Y.; Lippard, S. J. *Chem. Rev.* **2004**, *104*, 987–1011.
- (49) Que, L.; Tolman, W. B. *Angew. Chem., Int. Ed.* **2002**, *41*, 1114–1137.
- (50) Newcomb, M.; Toy, P. H. *Acc. Chem. Res.* **2000**, *33*, 449–455.
- (51) Pulver, S. C.; Froland, W. A.; Lipscomb, J. D.; Solomon, E. I. *J. Am. Chem. Soc.* **1997**, *119*, 387–395.
- (52) Lipscomb, J. D. *Annu. Rev. Microbiol.* **1994**, *48*, 371–399.
- (53) Nam, W. *Acc. Chem. Res.* **2007**, *40*, 522–531.
- (54) Fukuzumi, S.; Morimoto, Y.; Kotani, H.; Naumov, P.; Lee, Y. M.; Nam, W. *Nature Chem.* **2010**, *2*, 756–759.
- (55) Mayer, J. M. *Acc. Chem. Res.* **1998**, *31*, 441–450.
- (56) Balcells, D.; Clot, E.; Eisenstein, O. *Chem. Rev.* **2010**, *110*, 749–823.
- (57) Shaik, S.; Cohen, S.; Wang, Y.; Chen, H.; Kumar, D.; Thiel, W. *Chem. Rev.* **2010**, *110*, 949–1017.
- (58) Yoshizawa, K. *Acc. Chem. Res.* **2006**, *39*, 375–382.
- (59) Bathelt, C. M.; Zurek, J.; Mulholland, A. J.; Harvey, J. N. *J. Am. Chem. Soc.* **2005**, *127*, 12900–12908.
- (60) Shaik, S.; Kumar, D.; de Visser, S. P.; Altun, A.; Thiel, W. *Chem. Rev.* **2005**, *105*, 2279–2328.
- (61) Meunier, B.; de Visser, S. P.; Shaik, S. *Chem. Rev.* **2004**, *104*, 3947–3980.
- (62) Shaik, S.; Milko, P.; Schyman, P.; Usharani, D.; Chen, H. *J. Chem. Theory Comput.* **2011**, *7*, 327–339.
- (63) Noodleman, L.; Lovell, T.; Han, W. G.; Li, J.; Himo, F. *Chem. Rev.* **2004**, *104*, 459–508.
- (64) Baik, M. H.; Newcomb, M.; Friesner, R. A.; Lippard, S. J. *Chem. Rev.* **2003**, *103*, 2385–2419.
- (65) Siegbahn, P. E. M.; Borowski, T. *Acc. Chem. Res.* **2006**, *39*, 729–738.
- (66) Siegbahn, P. E. M.; Blomberg, M. R. A. *Chem. Rev.* **2000**, *100*, 421–437.
- (67) Basch, H.; Mogi, K.; Musaev, D. G.; Morokuma, K. *J. Am. Chem. Soc.* **1999**, *121*, 7249–7256.
- (68) Kumar, D.; de Visser, S. P.; Shaik, S. *J. Am. Chem. Soc.* **2004**, *126*, 5072–5073.
- (69) Johansson, A. J.; Blomberg, M. R. A.; Siegbahn, P. E. M. *J. Phys. Chem. C* **2007**, *111*, 12397–12406.
- (70) Silaghi-Dumitrescu, R. *New J. Chem.* **2010**, *34*, 1830–1833.
- (71) Balcells, D.; Raynaud, C.; Crabtree, R. H.; Eisenstein, O. *Chem. Commun.* **2009**, 1772–1774.
- (72) Hull, J. F.; Balcells, D.; Sauer, E. L. O.; Raynaud, C.; Brudvig, G. W.; Crabtree, R. H.; Eisenstein, O. *J. Am. Chem. Soc.* **2010**, *132*, 7605–7616.
- (73) Bloch, K. *Acc. Chem. Res.* **1969**, *2*, 193–202.
- (74) Abad, J. L.; Camps, F.; Fabriàs, G. *Angew. Chem., Int. Ed.* **2000**, *39*, 3279–3281.
- (75) Behrouzian, B.; Buist, P. H. *Curr. Opin. Chem. Biol.* **2002**, *6*, 577–582.
- (76) Fox, B. G.; Lyle, K. S.; Rogge, C. E. *Acc. Chem. Res.* **2004**, *37*, 421–429.
- (77) Buist, P. H. *Nat. Prod. Rep.* **2004**, *21*, 249–262.
- (78) Abad, J. L.; Camps, F.; Fabriàs, G. *J. Am. Chem. Soc.* **2007**, *129*, 15007–15012.
- (79) Shanklin, J.; Guy, J. E.; Mishra, G.; Lindqvist, Y. *J. Biol. Chem.* **2009**, *284*, 18559–18563.
- (80) Hummel, A.; Deleng, H. C.; Luthjens, L. H. *Radiat. Phys. Chem.* **1995**, *45*, 745–748.
- (81) Guallar, V.; Gherman, B. F.; Miller, W. H.; Lippard, S. J.; Friesner, R. A. *J. Am. Chem. Soc.* **2002**, *124*, 3377–3384.
- (82) Shaik, S.; de Visser, S. P.; Oglario, F.; Schwarz, H.; Schröder, D. *Curr. Opin. Chem. Biol.* **2002**, *6*, 556–567.
- (83) Shaik, S.; Cohen, S.; de Visser, S. P.; Sharma, P. K.; Kumar, D.; Kozuch, S.; Oglario, F.; Danovich, D. *Eur. J. Inorg. Chem.* **2004**, 207–226.
- (84) Shaik, S.; Hirao, H.; Kumar, D. *Acc. Chem. Res.* **2007**, *40*, 532–542.
- (85) Schley, N. D.; Blakemore, J. D.; Subbaiyan, N. K.; Incarvito, C. D.; D'Souza, F.; Crabtree, R. H.; Brudvig, G. W. *J. Am. Chem. Soc.* **2011**, *133*, 10473–10481.
- (86) Baciocchi, E.; Rol, C.; Sebastiani, G. V.; Serena, B. *Tetrahedron Lett.* **1984**, *25*, 1945–1946.
- (87) Blakemore, J. D.; Schley, N. D.; Olack, G. W.; Incarvito, C. D.; Brudvig, G. W.; Crabtree, R. H. *Chem. Sci.* **2011**, *2*, 94–98.

- (88) Hoertz, P. G.; Kim, Y.; Youngblood, W. J.; Mallouk, T. E. *J. Phys. Chem. B* **2007**, *111*, 6845–6856.
- (89) Zhao, Y.; Hernandez-Pagan, E. A.; Vargas-Barbosa, N. M.; Dysart, J. L.; Mallouk, T. E. *J. Phys. Chem. Lett.* **2011**, *2*, 402–406.
- (90) Pan, Z.; Horner, J. H.; Newcomb, M. J. *Am. Chem. Soc.* **2008**, *130*, 7776–7777.
- (91) Hirao, H.; Kumar, D.; Que, L.; Shaik, S. J. *Am. Chem. Soc.* **2006**, *128*, 8590–8606.
- (92) The weak complexes between the catalyst and the substrate that are identified on the pathways do not correspond to stable species on the Gibbs energy surfaces.
- (93) Gómez, L.; Garcia-Bosch, I.; Company, A.; Benet-Buchholz, J.; Polo, A.; Sala, X.; Ribas, X.; Costas, M. *Angew. Chem., Int. Ed.* **2009**, *48*, 5720–5723.
- (94) Hay-Motherwell, R.; Wilkinson, G.; Hussain-Bates, B.; Hursthouse, M. *Polyhedron* **1993**, *12*, 2009–2012.
- (95) Jacobi, B.; Laitar, D.; Pu, L.; Wargocki, M.; DiPasquale, A.; Fortner, K.; Schuck, S.; Brown, S. *Inorg. Chem.* **2002**, *41*, 4815–4823.
- (96) Balcells, D.; Raynaud, C.; Crabtree, R. H.; Eisenstein, O. *Chem. Commun.* **2008**, 744–746.
- (97) Balcells, D.; Raynaud, C.; Crabtree, R. H.; Eisenstein, O. *Inorg. Chem.* **2008**, *47*, 10090–10099.
- (98) Balcells, D.; Moles, P.; Blakemore, J. D.; Raynaud, C.; Brudvig, G. W.; Crabtree, R. H.; Eisenstein, O. *Dalton Trans.* **2009**, 5989–6000.
- (99) Siegbahn, P. E. M.; Crabtree, R. H. *J. Am. Chem. Soc.* **1999**, *121*, 117–127.
- (100) Siegbahn, P. E. M. *Curr. Opin. Chem. Biol.* **2002**, *6*, 227–235.
- (101) Lundberg, M.; Blomberg, M. R. A.; Siegbahn, P. E. M. *Inorg. Chem.* **2004**, *43*, 264–274.
- (102) Prokop, K. A.; de Visser, S. P.; Goldberg, D. P. *Angew. Chem., Int. Ed.* **2010**, *49*, 5091–5095.
- (103) Garcia-Bosch, I.; Company, A.; Cady, C. W.; Styring, S.; Browne, W. R.; Ribas, X.; Costas, M. *Angew. Chem., Int. Ed.* **2011**, *50*, 1–6.
- (104) Oglario, F.; Harris, N.; Cohen, S.; Filatov, M.; de Visser, S. P.; Shaik, S. J. *Am. Chem. Soc.* **2000**, *122*, 8977–8989.
- (105) Schöneboom, J. C.; Cohen, S.; Lin, H.; Shaik, S.; Thiel, W. *J. Am. Chem. Soc.* **2004**, *126*, 4017–4034.
- (106) Poli, R. *Chem. Rev.* **1996**, *96*, 2135–2204.
- (107) Poli, R.; Harvey, J. N. *Chem. Soc. Rev.* **2003**, *32*, 1–8.
- (108) Harvey, J. N.; Poli, R.; Smith, K. M. *Coord. Chem. Rev.* **2003**, *238*, 347–361.
- (109) Harvey, J. N. *Phys. Chem. Chem. Phys.* **2007**, *9*, 331–343.
- (110) Soucy, P.; Ho, T.; Deslongchamps, P. *Can. J. Chem.* **1972**, *50*, 2047–2052.
- (111) For the α C–H bond strength of THF, see: McMillen, D.; Golden, D. *Annu. Rev. Phys. Chem.* **1982**, *33*, 493–532.
- (112) For the tertiary C–H bond strength of isobutane, see: Blanksby, S.; Ellison, G. *Acc. Chem. Res.* **2003**, *36*, 255–263.
- (113) For a recent review on the homogeneity vs. heterogeneity problem in metal-catalyzed reactions, see: Crabtree, R. H. *Chem. Rev.* **2011**; DOI: 10.1021/cr2002905.
- (114) Castillo-Blum, S.; Richens, D.; Sykes, A. *Inorg. Chem.* **1989**, *28*, 954–960.
- (115) Karlsson, E. A.; Privalov, T. *Chem.—Eur. J.* **2009**, *15*, 1862–1869.
- (116) Bach, R. D.; Andres, J. L.; Su, M. D.; McDouall, J. J. W. *J. Am. Chem. Soc.* **1993**, *115*, 5768–5775.
- (117) Bach, R. D.; Su, M. D.; Aldabbagh, E.; Andres, J. L.; Schlegel, H. B. *J. Am. Chem. Soc.* **1993**, *115*, 10237–10246.
- (118) Doyle, M. P.; Duffy, R.; Ratnikov, M.; Zhou, L. *Chem. Rev.* **2010**, *110*, 704–724.
- (119) Schröder, D.; Shaik, S.; Schwarz, H. *Acc. Chem. Res.* **2000**, *33*, 139–145.
- (120) Shaik, S.; Filatov, M.; Schröder, D.; Schwarz, H. *Chem.—Eur. J.* **1998**, *4*, 193–199.
- (121) Truhlar, D. G.; Gao, J. L.; Alhambra, C.; Garcia-Viloca, M.; Corchado, J.; Sanchez, M. L.; Villa, J. *Acc. Chem. Res.* **2002**, *35*, 341–349.
- (122) Pu, J. Z.; Gao, J. L.; Truhlar, D. G. *Chem. Rev.* **2006**, *106*, 3140–3169.
- (123) Truhlar, D. G. *J. Phys. Org. Chem.* **2010**, *23*, 660–676.
- (124) The accurate calculation of KIE involving tunneling is complex and out of the scope of the present paper.
- (125) Lee, C. T.; Yang, W. T.; Parr, R. G. *Phys. Rev. B* **1988**, *37*, 785–789.
- (126) Becke, A. D. *J. Chem. Phys.* **1993**, *98*, 5648–5652.
- (127) Stephens, P.; Devlin, F.; Chabalowski, C.; Frisch, M. J. *Phys. Chem.* **1994**, *98*, 11623–11627.
- (128) Frisch, M. J. et al. *GAUSSIAN 03, revision D.01*; Gaussian, Inc.: Wallingford, CT, 2004.
- (129) Zhao, Y.; Truhlar, D. G. *Theor. Chem. Acc.* **2008**, *120*, 215–241.
- (130) Zhao, Y.; Truhlar, D. G. *Acc. Chem. Res.* **2008**, *41*, 157–167.
- (131) Frisch, M. J. et al. *GAUSSIAN 09, revision A.02*; Gaussian, Inc.: Wallingford, CT, 2004.
- (132) Andrae, D.; Häussermann, U.; Dolg, M.; Stoll, H.; Preuss, H. *Theor. Chim. Acta* **1990**, *77*, 123–141.
- (133) Bergner, A.; Dolg, M.; Küchle, W.; Stoll, H.; Preuss, H. *Mol. Phys.* **1993**, *80*, 1431–1441.
- (134) Hehre, W. J.; Ditchfield, R.; Pople, J. A. *J. Phys. Chem.* **1972**, *56*, 2257–2261.
- (135) Fukui, K. *Acc. Chem. Res.* **1981**, *14*, 363–68.
- (136) Hratchian, H. P.; Schlegel, H. B. In *Theory and Applications of Computational Chemistry: The First 40 Years*; Dykstra, C. E., Frenking, G., Kim, K. S., Scuseria, G., Eds.; Elsevier: Amsterdam, 2005; pp 195–249.
- (137) Ehlers, A. W.; Böhme, M.; Dapprich, S.; Gobbi, A.; Höllwarth, A.; Jonas, V.; Köhler, K. F.; Stegmann, R.; Veldkamp, A.; Frenking, G. *Chem. Phys. Lett.* **1993**, *208*, 111–114.
- (138) Höllwarth, A.; Böhme, H.; Dapprich, S.; Ehlers, A. W.; Gobbi, A.; Jonas, V.; Köhler, K. F.; Stegmann, R.; Veldkamp, A.; Frenking, G. *Chem. Phys. Lett.* **1993**, *203*, 237–240.
- (139) Hariharan, P. C.; Pople, J. A. *Theor. Chim. Acta* **1973**, *28*, 213–222.
- (140) McLean, A. D.; Chandler, G. S. *J. Chem. Phys.* **1980**, *72*, 5639–5648.
- (141) Raghavachari, K.; Binkley, J. S.; Seeger, R.; Pople, J. A. *J. Chem. Phys.* **1980**, *72*, 650–654.
- (142) Cramer, C. J.; Truhlar, D. G. *Acc. Chem. Res.* **2008**, *41*, 760–768.
- (143) Marenich, A. V.; Cramer, C. J.; Truhlar, D. G. *J. Phys. Chem. B* **2009**, *113*, 6378–6396.
- (144) Reed, A. E.; Curtiss, L. A.; Weinhold, F. *Chem. Rev.* **1988**, *88*, 899–926.
- (145) Harvey, J. N.; Aschi, M.; Schwarz, H.; Koch, W. *Theor. Chem. Acc.* **1998**, *99*, 95–99.